Idiosyncratic Functions of Active Touch Strategies in Shape Perception.

Neomi Mizrachi (neomi.mizrachi@weizmann.ac.il)
Weizmann Institute of Science
Guy Nelinger
Weizmann Institute of Science
Ehud Ahissar
Weizmann Institute of Science
Amos Arieli
Weizmann Institute of Science

Research Article

Keywords: Idiosyncratic Functions , Shape Perception, Hand movements, physiological parameters

Posted Date: May 25th, 2021

DOI: https://doi.org/10.21203/rs.3.rs-537011/v1

Title: Idiosyncratic functions of active touch strategies in shape perception.

Abbreviated title: Active touch strategies underlying shape perception.

Authors names and affiliations: Neomi Mizrachi [^#], Guy Nelinger [#], Ehud Ahissar [^#*], Amos Arieli [^#*]

[#] Neurobiology department, Weizmann Institute of Science, 7610001 Rehovot, Israel

[*] Equal contribution

^ Corresponding author.

Corresponding authors email addresses: Ehud Ahissar ehud.ahissar@weizmann.ac.il

Amos Arieli amos.arieli@weizmann.ac.il Neomi Mizrachi neomi.mizrachi@weizmann.ac.il

Number of pages: 40

Number of figures: 5

Number of tables: 1

Number of words for abstract: 145

Number of words for introduction: 315

Number of words for discussion: 1453

ABSTRACT

Hand movements are essential for tactile perception of objects. However, the specific functions served by active touch strategies, and their dependence on physiological parameters, is unclear and understudied. Focusing on planar shape perception, we tracked at high resolution the hands of eleven participants during shape recognition task. Two dominant hand movements strategies were identified: Contour-following movements, either tangential to the contour or oscillating perpendicular to it, and exploration by scanning movements, crossing between distant parts of the shapes' contour. Both strategies exhibited non-uniform coverage of the shapes' contours. Idiosyncratic movement patterns were specific to the sensed object and could be explained in part by spatial and temporal tactile thresholds of the participant. Using simulations, we show how some strategy choices may affect receptors activation. These results suggest that motion strategies of active touch adapt to both the sensed object and to the perceiver's physiological parameters.

SIGNIFICANCE STATEMENT

Hand movements are integral components of tactile perception. Yet, the functions of the specific motion strategies used to perceive physical shapes are not clear. Focusing on planar shape perception and using high-speed hand tracking we show that human participants employ two basic hand-movement strategies: Contour-following and scanning. We further show that the strategy chosen by each participant and its kinematics depend on the shape of the sensed object and on idiosyncratic physiological thresholds, thresholds that are indicative of the participant's spatial resolution and temporal adaptation dynamics. These results describe the active-touch strategies underlying shape perception and provide insights into the functional advantages obtained by their idiosyncratic selection.

INTRODUCTION

Perception usually co-occurs with sensors' movements [1–10]. Moreover, in primates, it has been established that hand movements are an integral component of tactile perception of objects'

features [8,11–19]. Yet, the nature of these movements and their dependency on other perception-relevant factors are not sufficiently characterized. In a seminal series of studies, Lederman, Klatzky and colleagues introduced the first comprehensive description of active "Exploratory procedures" (EPs) of 3D objects – stereotyped movement patterns having invariant characteristics. Thus, for example, 'Pressing' was found to be the primary EP for evaluating hardness, 'Lateral motion' for evaluating texture and 'Contour-following' (*CF*) for evaluating the shape of 3D objects [8]. *CF* variants were further analyzed in consequent studies [20–22].

Initial quantitative studies of planar (2D) objects revealed that humans adapt their movement patterns to the spatial characteristics of the scanned surfaces; speed, for example, is adjusted to spatial frequency [14] and direction to the spatial orientation of the surface's texture [23,24]. Such adaptations evolve through development [25], can be acquired via consequent exposures to specific features [24,25] and can be directly taught [14]. In these studies, the adaptations resulted in maintaining specific sensory cues in a given "working range", likely optimal for sensation, consistent with principles of closed-loop control [11,26–28]. Similar maintenance of "controlled variables" has been observed in other tactile tasks, both in humans and rodents [17,29–31].

Overall, studies on active touch have been providing convincing evidence that hand movements are an integral part of tactile perception. Yet, the principles that determine hand movement patterns and their idiosyncratic functions are not known. In the present study we use a simple tactile identification task of planar (2D) shapes to address these questions. The use of planar shapes allowed for a highly detailed examination of hand trajectories. We first characterized the repertoire of hand movements among human participants and then investigated their dependencies on idiosyncratic sensory physiology.

RESULTS

Overall, 18,701s of hand movements were recorded at high resolution from 11 human participants while performing tactile recognition task of planar shapes (1,196 trials in total). Separate finger movements were prevented by binding together the three palpating fingers (Fig. 1A). In order to generalize the results over the types of tactile items, two sets of tactile items were used - Objects (further divided to set A and set B) and Features (further divided to sets of Angle, Tilt and Curvature, Fig. 1B). In order to generalize over differences in idiosyncratic experience, three patterns of item-presentation orders were employed.

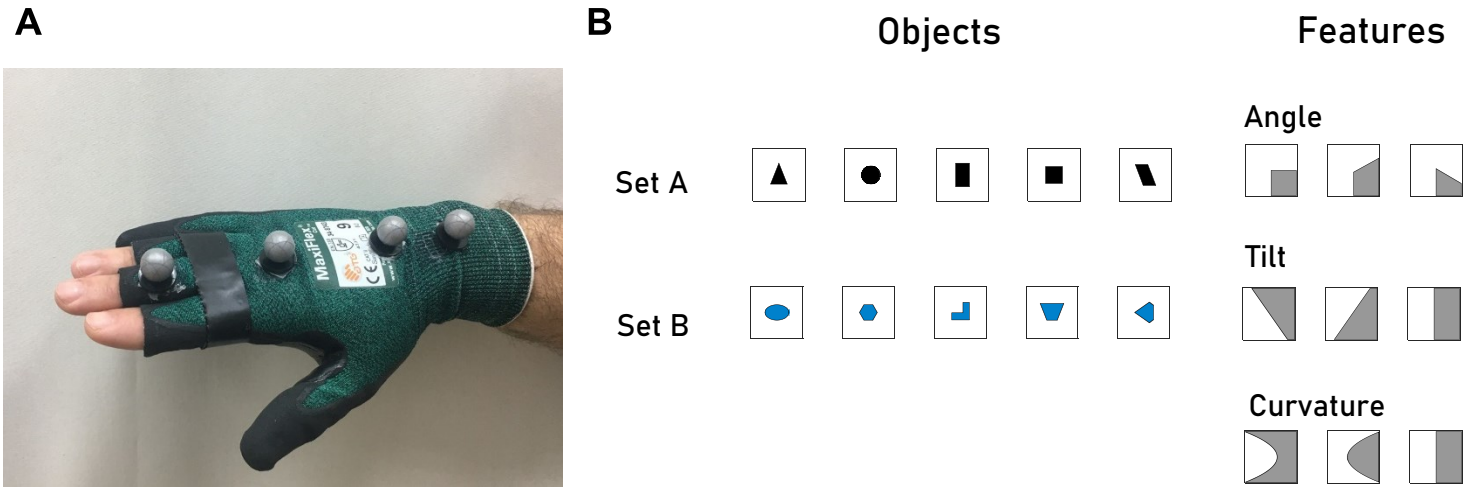

Figure 1. Recording and tactile items. (A) The glove used with four designated Vicon markers attached to it. Two markers were attached above the wrist carpal bones and two above the middle finger's middle and proximal phalanges. (B) Tactile items. Two sets of tactile items were used: Objects (left) and Features (right). Objects were divided into set A (top, black) and set B (bottom, blue). Features were divided into three blocks: Angle (left), Tilt (middle) and Curvature (right). For all tactile items, the colored area was raised by 25 μm relative to the background area.

Contour-following and scanning are two common procedures for planar shape recognition

In each trial, the trajectory of the hand was superimposed on the outline of the shape. The degree of time spent in the contour vicinity differed substantially across trials (Fig. 2A-C). Using a geometrical algorithm we quantified the degree of coverage of the inner part of the shape area and the time spent in the contour vicinity (Fig. 2A right, black and blue areas, respectively; see Materials and Methods). Approximately half of the trajectories did not cross between the shape contours while the remaining did (52% and 48%, respectively). In trials in which the trajectory did not cross the shape center, typically, most of the trial time was spent in the contour vicinity (Fig.2A, right). Based on this analysis we have categorized the trajectories into two major classes: Contour-following (*CF*), where the trajectory mostly followed the shape's outline and did not cross between them, and Scanning (*Sc*), where the trajectory either crossed between distant parts of the shapes' contour or when a large portion of the trial time ($\geq$ 25%) was spent far from the contour vicinity (Fig. 2A, left, red; see Materials and Methods). *CF* trajectories were sub-classified as *Linear* (Fig. 2B ,left) and *Oscillating* (Fig. 2B, middle); trials could include one sub-class (Fig. 2B, left, middle) or both (Fig. 2B , right). *Sc* trajectories exhibited different degrees of shape coverage and different foci (Fig. 2C). On average *Sc* trials differed from *CF* in their kinematics: *Sc* trials were characterized by higher tangential (scanning) speeds, longer traveled distances, higher entropy and higher speeds along the z-axis (perpendicular to the scanned surface) (Fig. 2D, $p<0.0005$ for all differences). These strategy types and sub-types were exhibited for all objects and during all sessions tested in this study (Supplementary material, Fig. 1).

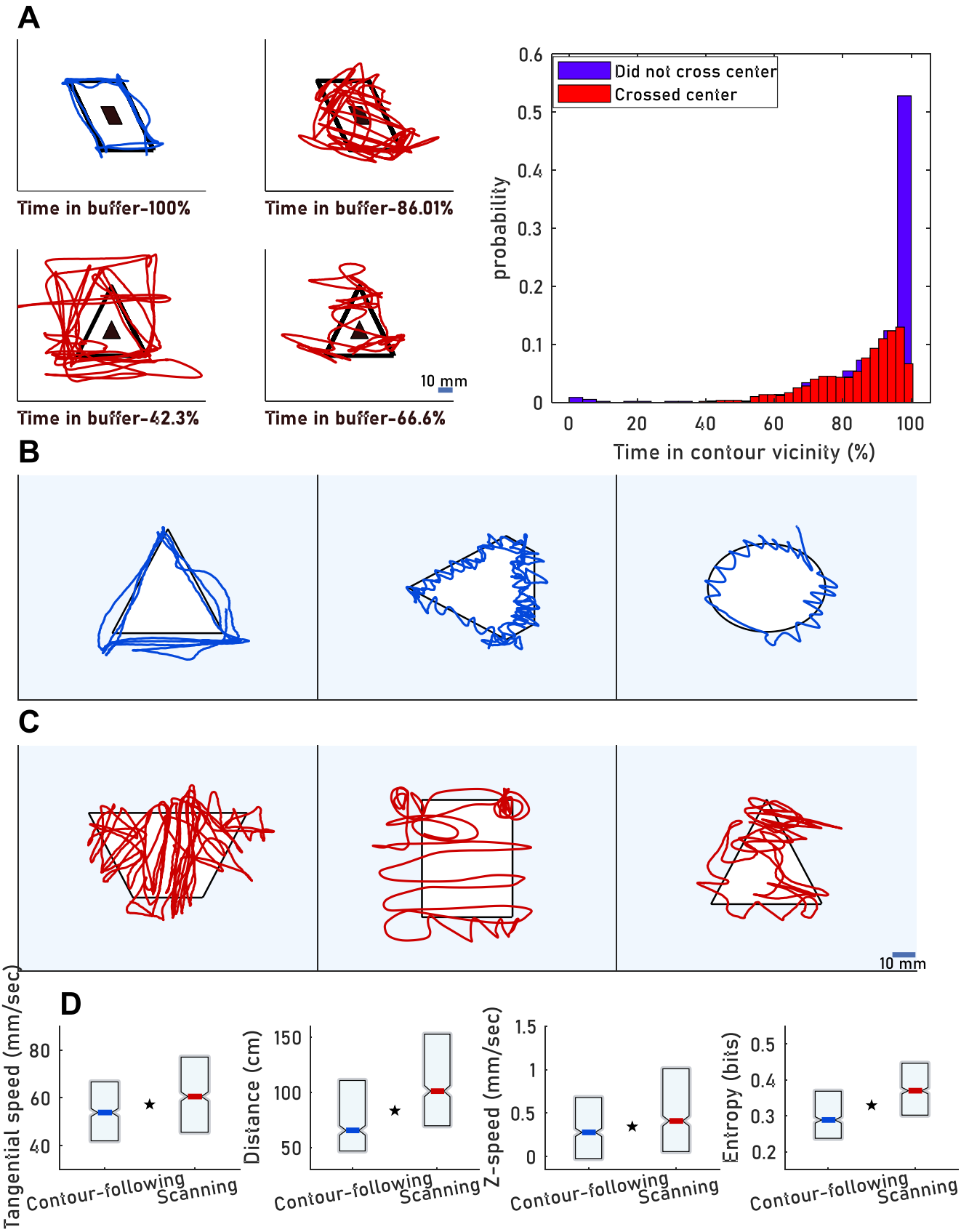

Figure 2. Classes of motor patterns. (A) Left: Classification of individual trials was based on the degree of time spent in the shape center (left, small black shape) and in the contour vicinity (left, blue buffer between the inner and outer guiding shapes) (see Materials and Methods). Examples of *CF* trials (left, blue) and *Sc* trials (left, red) are depicted. Right: probability of the time spent in the contour vicinity based on whether the shape center was crossed or not. (B) *CF* trials were sub-classified as '*Linear*' (left) '*Oscillating*' (middle) or both (right). (C) Examples of various manifestations of *Sc* trials; common scale bar (C, right) for all panels. (D) Distributions (medians and quartiles) of four kinematic variables across all *CF* and *Sc* trials ($p<0.0005$ for all differences). $N_{subjects}= 11$; $N_{Sessions} = 51$ (4-5 sessions per participant); $N_{trials}= 1196$. $N_{CF\ trials}$: 537. $N_{-Sc\ trials}$: 659.

Focal palpation

A focal index (see Materials and Methods) was used to evaluate the degree in which the participants exhibited non-uniform coverage of the shapes' contours, focusing on specific parts of the explored shape (e.g., the part surrounded by a pink circle, Fig. 3A). *Sc* trials' median focal index was significantly higher than that of the *CF* trials (Fig. 3B, $p<0.0005$). This difference was evident for all objects of Sets A and B (Fig. 3C). A significant correlation was observed between the median focal index and the object's sharpest angle (excluding the circle and ellipse) for *CF* trials (Fig. 3D, $r = -0.86$, $p = 0.006$, adjusted alpha level = 0.016; 0.05/3), but not for *Sc* trials ($r = -0.69$, $p = 0.057$, $r_{Spearman} = -0.65$, $p_{Spearman} = 0.08$, adjusted alpha level = 0.016; 0.05/3). No significant dependency was found ($p=0.33$) between the focal index (per participant) and the order or type of items presented. Example trajectories of the objects with the highest or lowest sharpest angle (triangle and hexagon, respectively) are depicted in Fig. 3E. Visit rates (see Materials and Methods) of two objects (Triangle and L shape), demonstrating the focus of specific shape regions, are depicted in Fig. 3F.

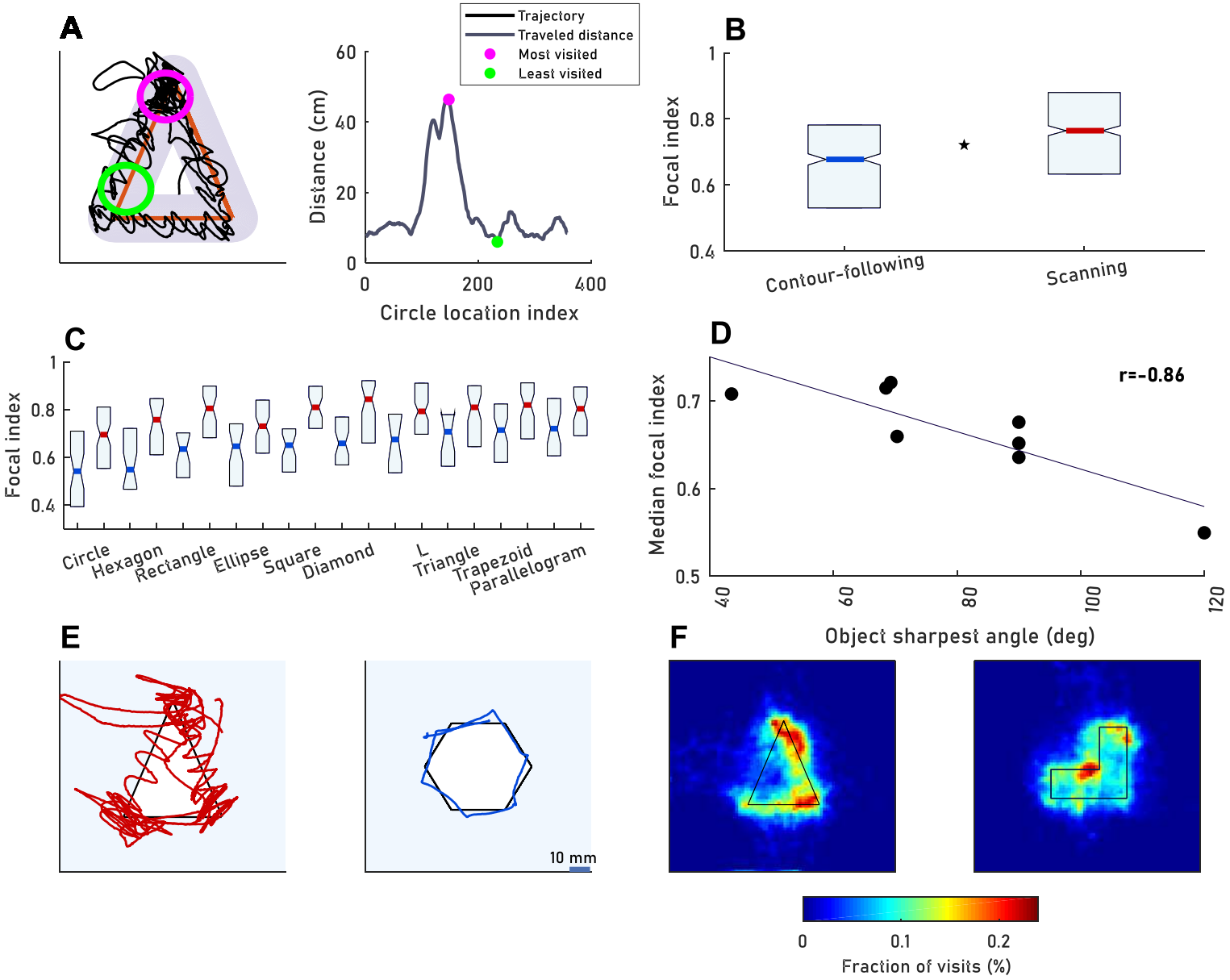

Figure 3. Focal palpation. (A) An example demonstrating the calculation of a trial's focal index. Left: overlapping circles with a radius of 10 mm (gray) were plotted over the objects' outline (red). The traveled distance in each circle was calculated. Circles with the maximal and minimal value of traveled distance (pink and green, correspondingly) are marked. Right: Calculated traveled distance (y-axis) as a function of the location of the circle's center (x-axis). The trial's focal index is defined as the ratio of the difference between the trial's maximal and minimal values of traveled distance (pink and green) and their sum. (B) The distributions (medians and quartiles) of the focal index for *CF* and *Sc* trials across all trials of all participants and all sessions (henceforth "grand distributions") ($p<0.0005$). Ns of subjects, sessions and trials are as specified in figure 2D. (C) Grand distributions of the focal index per object in *Sc* and *CF* trials. (D) Each data point represents the object grand median focal index and the object sharpest angle for *CF* trials. Objects' sharpest angle: Triangle=43.5°, trapezoid= 68.2° , parallelogram=69.2°, diamond=70.3°, square, rectangle, L shape=90°, hexagon=120°.$N_{\text{trials per shape}}$, panels B-D: Triangle, 70; Circle, 128; Rectangle, 68; Square, 83; Parallelogram, 80; Ellipse, 121; Hexagon, 66; L, 104; Trapezoid, 117; Diamond, 95. (E) Examples of two trajectories differing in their focal indices (Triangle, focal index (FI) = 0.77; Hexagon, FI = 0.34). (F) Mean visit rates for two example objects (triangle and L, all subject and trial types included).

Trajectories are idiosyncratic and depend on the explored shape

Previous studies described a repetition of eye movement's trajectories in subsequent views of the same picture [32–36]. In order to test whether such repetition appears in hand movements we computed a similarity index for every pair of trials of a single participant when they explored the same shape (see Materials and Methods). Similarity index values ranged between - 0.93 to + 0.96, exhibiting a bias towards positive correlations (mean ± SEM: 0.06 ± 0.003, $p<0.0005$). Two examples of strong and one example of typical positively correlated trajectories are depicted in Figure 4A. These examples demonstrate that, as expected, the component that dominated the trial-to-trial similarity was the slow component of palpation; the rapid oscillations around the contours were typically not correlated across trials. The mean similarity indices of participants exploring the same shape were significantly higher than the indices of a random normal distribution, indices of the same participant exploring different shapes, or indices of different participants exploring the same shape (Fig. 4B, $p<0.0005$ for all differences). Similarity indices did not differ between *Sc* and *CF* trials ($p>0.05$). Similarity indices for the first half of each trial were significantly higher than those for the second half (Fig. 4C; $p=0.005$, signed rank test). This difference is in line with previous reports, suggesting that initial eye movement patterns were replicated more often [37,38]. Between session I and III the similarity indices computed for the first half of the trials significantly increased ($p=0.048$, signed rank test), suggesting that with practice, initial movements became more stereotyped. No significant dependency of participants' similarity indices on the order or type of objects presented was found ($p=0.41$).

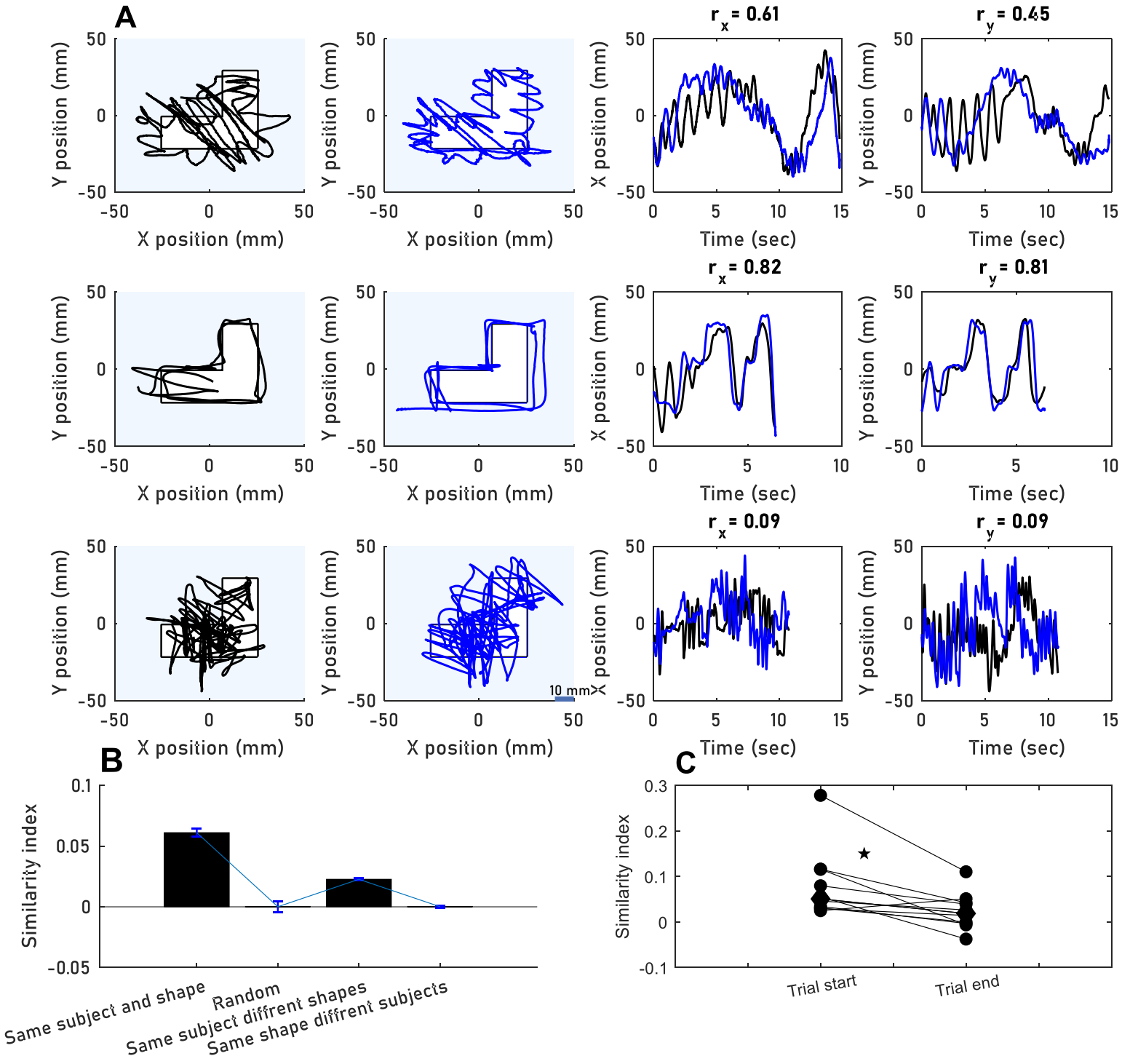

Figure 4. Idiosyncratic hand movements. (A) Three examples of three subjects' hand trajectories while they explored the same shape. Top, subject EV; middle: subject AG, bottom, subject AS. Left: x-y plots for two sequential trials with the same object. Right: x and y projections as a function of time, with the two trials superimposed after appropriate down sampling (see Materials and Methods). (B) Mean similarity indices (mean ± SEM across participants, see Materials and Methods) for subject-shape pairs and control pairs. (C) Each data point represents the median similarity index of one participant in either the first half of the trial or the second. First half median values were significantly higher ($p=0.005$).

Palpation speed correlates with the participant's idiosyncratic spatial resolution

With adaptive active sensing it is expected that scanning velocities are tuned to optimize receptor activation. It has been shown that primates prefer hand movement patterns that preserve certain temporal cues [13,14,23,24,39], cues whose temporal frequencies best fit one class of mechanoreceptors in the fingertip [40–43]. Hence, adaptive active sensing predicts that variations in hand speeds across participants should correspond to variations in the spatial spacing of their receptors. In this case, the temporal frequencies of activation will be preserved in the preferred working range by the finger speed, as the temporal frequency generated on the skin when scanning a single edge is determined by the multiplication of the finger speed and the spatial frequency of receptors across the skin [44]. To test for this possibility, we measured the Just-Noticeable-Difference (JND) in the index, middle and ring fingers of 10 of our participants (see Materials and Methods), as an indicator of the spatial spacing of the receptors array.

Consistent with previous reports [45], JND values (JND = 3.16 ± 0.98) varied substantially across our participants. Importantly, for each participant the three tested fingers had similar JND values (table 1, last column). During their first session, the median tangential speeds of the participants were correlated with the mean JND measured across the three fingers (Supplementary material, Fig. 2B, r = 0.74, p= 0.014, adjusted alpha = 0.0056; 0.05/9). The correlations were high for the JNDs of the middle (Fig. 5A, r= 0.84, p =0.0026; adjusted alpha level = 0.0045; 0.05/11, r - 95% confidence range [0.6,0.89], p - 95% confidence range [0.0005,0.06], see Materials and Methods) and index fingers and somewhat weaker for the ring finger (Supplementary material, Fig. 2 A,C, Index finger: r = 0.725, p = 0.017, Ring finger: r =0.43, p =0.21, adjusted alpha = 0.0056; 0.05/9). Although participants could use any part of the three fingers array (we did not measure the movement of individual fingers), it is possible that the middle and index fingers were used more often than the ring finger, as previously reported in softness discrimination tasks [16,46]. A less frequent use may account for the weaker

157 correlation of the ring finger. No significant dependency of participants median tangential
158 speeds on the order or type of objects presented was found ($p = 0.28$).

159 In order to assess the dependency of this correlation on the known unreliability of the two-
160 point discrimination method (see Discussion), we have conducted a bootstrap test that covers,
161 statistically, the estimated range of unreliability [47] (see Materials and Methods). The bootstrap
162 analysis shows that the correlation coefficient (r) could rarely be < 0.5, and only in 8.1% of the
163 cases one would get $p > 0.05$ (Fig. 5A, right). We thus assume that the finding of a positive
164 significant correlation between the participants' tangential speed and their mean JND is robust.

165 The temporal frequency of activation of adjacent mechanoreceptors equals the scanning
166 speed divided by receptor spacing [44]. The positive correlation observed between the
167 participants' median speed and their JND may be consistent with an attempt to maintain this
168 temporal frequency within a narrow range [48]. Indeed, in session I, the participant-specific mean
169 frequencies ranged between 12.8 and 22.9 Hz (15.95 ± 3.18). The mean evaluated activation
170 frequency and its range increased monotonically along consequent sessions (Middle-finger,
171 Mean evaluated activation frequency: Ses1: 15.9 ± 3.18, Ses2: 17.07 ± 5.26, Ses3: 18.12 ±
172 4.9, Ses4: 18.14 ± 6.38, Range of activation frequencies: Ses1: 10.14, Ses2:19.2, Ses3:
173 15.45, Ses4: 22). The mechanoreceptor type that is most sensitive in the range of our
174 evaluated activations frequencies in session I (between 12.8 and 22.9 Hz) is the rapidly
175 adapting (RA) [42]. To test the potential effects of JND-dependent speed modulations on
176 neuronal activations, we simulated the responses of grids of RA units with varying densities
177 using the TouchSim computational model [49] (see Materials and Methods, Supplementary
178 material, Fig. 2). The simulation shows that the scanning speeds, used by our participants in
179 session I (between 34.4 to 77.14 mm/sec) generate activation rates within a narrow range
180 (Fig. 5B, range between vertical dashed lines). We compared the speed range used by our
181 participants to different speed values using equal size windows (50 mm/sec), across the
182 simulation speed values. The window containing our participants speed values (30-80
183 mm/sec) allowed for significantly higher spike rates than in other equal size windows (3.99 ±

184 0.008 spikes/sec versus 3.73 ± 0.22 spikes/sec, p=0.004). The mean variability between
185 neighboring neurons was significantly lower in this window in comparison to the other windows
186 (0.05 vs. 0.32 spikes/sec, p< 0.0005, Fig.5C).

Participant	Index finger JND (mm)	Middle finger JND (mm)	Ring finger JND (mm)	Mean JND (mm)
AF	3	2	2	2.33 ± 0.57
EV	3	3	4	3.33 ± 0.57
MF	4	5	5	4.66 ± 0.57
AS	3	4	4	3.66 ± 0.57
YB	4	3.5	4	3.83 ± 0.28
SG	5	5	6	5.33 ± 0.57
DR	4	3	3.5	3.5 ± 0.5
HA	4	4	4	3.5 ± 0
MG	2	3	3	2.66 ± 0.57
ZA	3	2	3.5	2.83 ± 0.76

Table 1. Two-point discrimination JND per participant: JND values in a static two-point discrimination task in the pads of the middle, index and ring fingers, and mean values across these fingers.

187 **Palpation curvature inversely correlates with the participant's idiosyncratic sensory**
188 **adaptation time**

189 One of the major differences induced by the *Linear* and *Oscillating* sub-classes of *CF* (Fig.
190 2B) was in the duration of continuous interactions between the fingertip and the shape's edge.
191 *Linear* motion induced longer epochs of such interactions than *Oscillating* motion.

192 A natural physiological feature that might be related to the choice between these strategies
193 is the receptor adaptation rate. Receptors with slower adaptation processes allow longer
194 epochs of similar stimulation and longer *Linear* motions. We have thus tested the effective
195 adaptation times of our participants, while following edges of different line types (straight, tilted
196 or curved) or following straight lines at different heights (see Materials and Methods).
197 Participants were asked to follow outlines, forward and backward, for 30 sec. For each trial,
198 the trajectory of the hand was analyzed and the time that elapsed from trial onset to the first

deviation of the trajectory from the outline was considered as the adaptation time of that trial (Supplementary material, Fig. 2) .The mean adaptation time of a participant (T_a) was calculated across all her or his adaptation trials (see Materials and Methods). In order to examine if curvier *Oscillating* motion indeed prolonged the effective adaptation time, we compared the adaptation times of our participants when following the shape's outline using *Oscillating* and *Linear* motions (Experiment B). The adaptation times were longer with *Oscillating* motion for most of the participants (Mdn $_{Oscillating}$ = 29.07 sec, IQR $_{Oscillating}$ = 30-26.3 sec vs Mdn $_{Linear}$ = 22.90 sec, IOR $_{Linear}$ = 29.8-17.3 sec; signed rank = 9, p = 0.12, signed rank test; Fig. 5D). To estimate quantitatively the pattern of *CF*, we computed the curvature index for every trial (Fig. 5E). During the first session, the correlation between the participants' T_a (22.29 ± 8.02, N =10 participants) and their curvature index (0.26 ± 0.14) was high (Fig.5F, r = -0.77, p = 0.0095, adjusted alpha = 0.01; 0.05/5). Thus, naïve participants with shorter adaptation times used curvier movements, such that they increased the number of border crossings and shortened the epochs in which skin stimulations remained relatively constant. No significant dependency was found between the participants' median curvature indices and the order or type of the presented items (p = 0.16).

To test the potential effects of *Linear* and *Oscillating* motion on neuronal activations, we simulated the responses of a grid of RA units to these motion types, using the TouchSim computational model [49] (see Materials and Methods). The simulation confirmed the prediction that employment of *Oscillating* motion induces more synchronous firing and an overall higher spike rate per neuron (p<0.0005) than *Linear* motion (Fig. 5G). RA firing was triggered by both the onset and offset of tactile stimulation, simulating the indentation induced by contour scanning (see Materials and Methods). While the intensity of RA firing could be controlled by their pressing force, the timing was controlled by the scanning trajectory – the curving of the scanning trajectory was adapted by our participants according to their adaptation times (Fig. 5F).

The correlations between motion strategies and sensory thresholds diminish with practice

In the three sessions that followed the first session, the curvature index and the hand speed gradually lost their dependence on the participant's T_a or JND (Fig. 5H, supplementary material, Fig. 2D). The decrease in correlation may result from transient, practice-induced changes in relevant physiological thresholds as previously reported [50], from changes in strategy (for example, hand speed was shown previously to depend on the stimulus or the task [14,51,52]) , or from both. Practice-induced strategy changes are supported in our study by the changes in preference for *CF* versus *Sc* palpation observed across sessions, as well as by differences in visit-rate patterns that depended on their practice history (Supplementary material, Fig. 3).

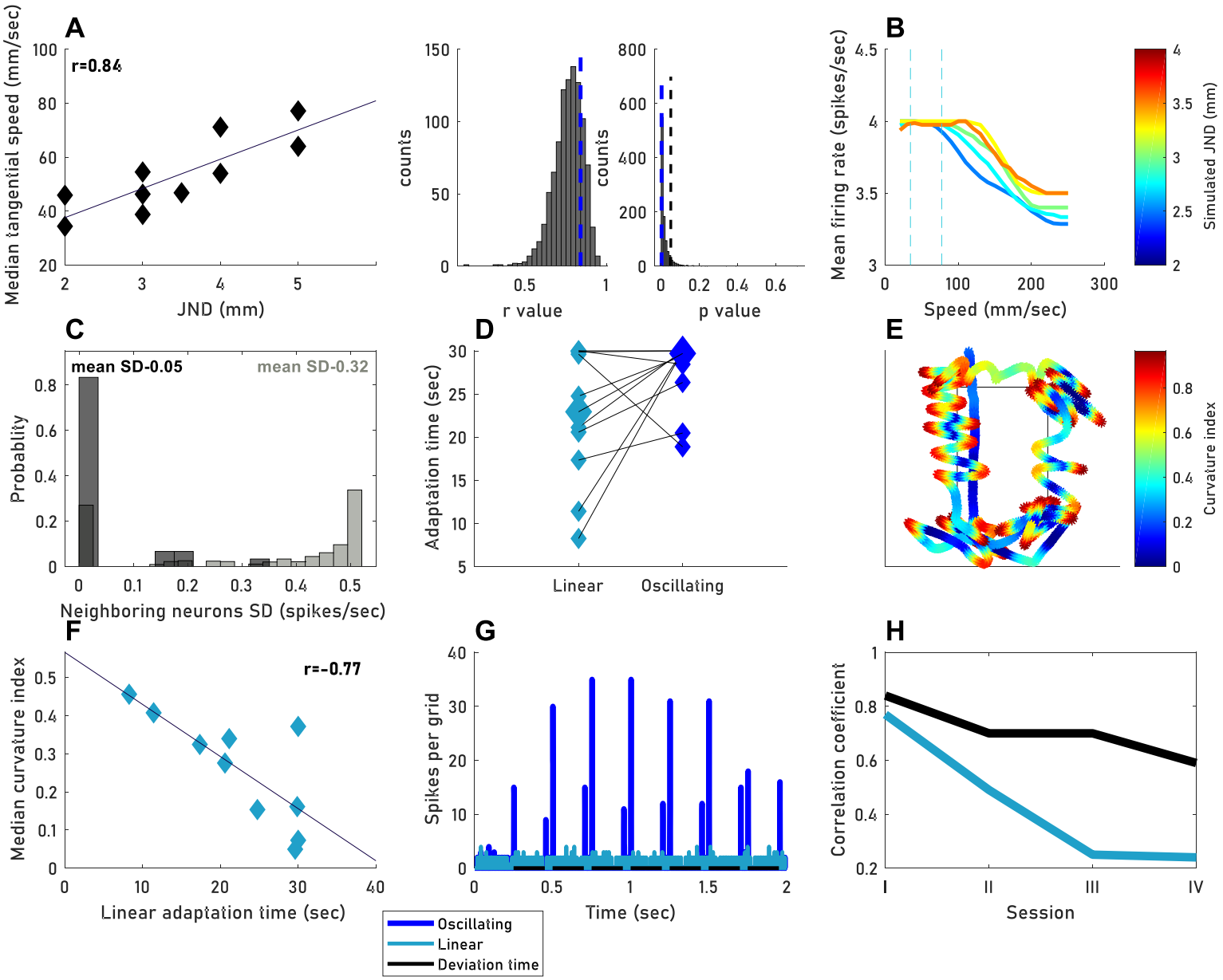

Figure 5. Dependency on sensory thresholds. (A) Left: Each data point represents the median tangential speed (across all trials of the first session) and the middle finger JND of one participant (18-29 trials per participant). Right: Probability distributions of r and p values across a bootstrap sample (N = 1000) of possible JND values, assuming known unreliability of JND measurements (see Materials and Methods). Experimental r and p values are marked by the dashed blue lines. Black vertical dashed line represents p = 0.05. (B, C) TouchSim simulations (see Materials and Methods). (B) The mean number of spikes per neuron plotted against tangential speed. Color code represents the distance between units in the grid (2-4 mm). The range of speed used by our participants is marked by the dashed gray lines. (C) Histogram of SD values between firing rates of neighboring neurons, for either the window containing speed values used by our participants (dark gray) or all other equal-size windows (light gray). (D) Each two connected data points represent one participant's mean adaptation time (Ta) using *Linear* (light blue) or *Oscillating* (blue) motion (11 Linear and 11 Oscillating trials per participant). Median values for each motion type are represented by a larger shape (median Ta Oscillatory= 29.07, median Ta Linear= 22.9 sec). (E) Curvature approximation. The curvature index (see Materials and Methods) during one example trial is color coded along the trajectory. (F) Each data point represents the median curvature (across all trials of the first session) and the mean *Linear* Ta of one participant (4-24 *CF* trials per participants). (G) Number of spikes for a grid of RA units for either *Oscillating* (blue) or *Linear* (light blue) motion. The time of deviation from the contour, in *Oscillating* motion, is marked in black. (H) Black: Correlation coefficient between JND and tangential speed per session. Light blue: Absolute value of the correlation coefficient between the curvature and adaptation time per session. N = 10 participants, for all panels.

DISCUSSION

This study describes the repertoire of hand movements strategies employed by human participants when required to recognize planar (2D) object shapes. Consistent with previous studies of 3D shapes [8,20,21], we found that one major strategy was Contour-Following *(CF)* – participants moved their fingers along the contours of the shape. In addition, we found a second major strategy – Scanning (*Sc*) – with which participants used large movements crossing the entire shape. Both strategies, and in particular *Sc,* included focal scanning of specific object regions. *CF* was employed in two major patterns – *Linear* and *Oscillating* motion. At subsequent exploration of the same shape, participants' movement trajectories were correlated. Such that the same locations on the shape were visited in the same relative time. This result is in line with the similarity in eye movements' trajectories previously reported [33–36,53].High-resolution tracking of hand movements revealed a strong dependency of critical movement parameters on two physiological thresholds – a spatial (JND) and temporal (T_a) ones. When the participants were naïve to the task, their tangential velocities were correlated with their fingertip spatial resolution and their tendency to perform an *Oscillating* motion variant of *CF* was correlated with their mechanosensory adaptation time. These correlations gradually decreased with practice. One interpretation of these results is that, with practice, human participants adapt scanning strategies that compensate for their sensory limitations.

Taken together, these results provide a detailed description of the specific hand movement strategies used for shape perception and open a window to the complex ways in which individual sensory abilities, practice repertoire and task-demands converge to an effective motor-sensory exploration strategy.

Experimental constraints

We attached the three palpating fingers (index, middle and ring) together, in order to be able to measure all motion components that are relevant to the perception of the objects. The participants were free to use any part of the affected sensory array, which was included the contact areas of the three fingertips. Thus, in a way, the three fingers were treated as one

large finger. As far as it is known from the literature, tactile perception naturally involves coordinated motion of all contacting fingers: Participants' fingers were shown to have correlated positions and speeds in tactile search tasks [54] as well as in a task designed to require only one finger [55]. Even when human participants were specifically instructed to use only one finger, low amplitude, correlated movements were seen in the other fingers [56]. Nevertheless, in the current study we did not examine the independent movement of each finger, a degree of freedom that might be treated differently by different participants.

Traditionally, two methods have been used to assess the spatial tactile resolution in specific skin areas of specific subjects: two points discrimination [57–59] and grating orientation task [60]. Here we used the former method. In order to generalize our results across these methods we have computed our confidence levels based on the comparison between these two methods. Participants' JND values were adjusted using values randomly picked from a distribution of differences between the two methods [47]. The adjusted JND values were compared to participants' median speeds. The resulting r and p values adopted from these comparisons were used to estimate the confidence range of the relation between JND and speed (Fig. 5A, see Materials and Methods).

Exploratory procedures of shape perception

In a pioneering study, Lederman and Klatzky termed the concept "Exploratory Procedures" (EPs) to refer to the motor-sensory exploration strategies characterizing the palpation of various classes of 3D objects under specific tasks [8]. Here we zoomed into a one class of objects – planar shapes – and tried to characterize the EPs that are naturally employed by human participants when asked to identify shapes. Our results expand those of Lederman and Klatzky and their collaborators [8,20,21] by showing that people employ not only *CF*, as observed by these researchers, but also *Sc* motions, when exploring shape in 2D objects (Fig. 2). The *Sc* motion resembles the 'Lateral-motion' EP, which was reported as the dominant strategy for texture palpation in 3D objects [8].

289 Our high-resolution tracking system provided additional information about the nature of these
290 strategies, revealing that human participants vary in the specific pattern of each EP – *Linear*
291 and *Oscillating* motions for *CF* and uniform and non-uniform coverage of the shapes' contours
292 for both the *Sc* and *CF*. Our tracking also revealed a frequent use of a palpation policy that
293 was not describe before – focal palpation. Participants often dedicated a significant portion of
294 time to explore specific regions of the objects. Focal palpation was more evident in *Sc* trials,
295 (Fig. 3) and depended on the properties of the explored object: Objects with sharp angles
296 were explored in a more focal manner. The tendency to use focal palpation was hardly affected
297 by the participants' physiological thresholds. Focal palpation was recently reported to
298 frequently occur when blindfolded sighted human subjects explore objects (2D and 3D) using
299 an active sensory substitution device [61]. Interestingly, such focal palpation was typically not
300 observed with blind subjects exploring the same objects with the same device – their palpation
301 covered the explored objects more uniformly. It thus seems that, in sighted subjects, focal
302 palpation results from, or uses, the accumulated experience of perceiving similar objects
303 visually.

304 **Sensation-dependent movements, controlled variables and closed-loop touch**

305 Sensory-motor behavior depends on the physiological parameters of sensory receptors [62,63].
306 Consistently, our results clearly demonstrate that the choice of motion strategy depends
307 strongly on sensory physiology. The speed of motion decreased with increased spatial
308 resolution (reduced JND) at the fingertip, and the degree of motion curvature increased with
309 faster adaptation times (T_a, Fig. 5). These correlations were very strong when our participants
310 were naïve to the task: During session I, the physiological measures, JND and T_a, could
311 explain 70% and 59% of the variability in the tangential speed and curvature index,
312 respectively. Such behavior is expected when the tactile system is concerned with maintaining
313 specific sensory variables in their "working ranges", i.e., ranges that allow satisfactory
314 perception [26,41,64]. Thus, rats maintain head azimuth and whisker speed [30] and humans

maintain hand coordination and hand speed when localizing objects around them [17] and ocular drift speed when viewing simple 2D shapes [65].

When scanning planar objects via touch, humans also often attempt to maintain temporal activation variables within certain ranges. Thus, humans, when perceiving textures, reduce hand speeds with higher external spatial frequencies, such as to maintain the temporal frequencies within a limited range [14]. When exploring surfaces with different geometry and friction attributes, they modify radial and tangential forces, together with lateral hand speeds, such as to maintain a certain amount of skin deformations [31]. Maintaining such sensory signals within certain ranges is expected to facilitate their predictive processing within brain circuits [26,66–68]. Variables that are actively maintained within specific ranges are termed "controlled variables" [64,69–71]. Preserving them in preferred working ranges requires a closed-loop architecture, in which the variables can be sensed and manipulated. As these controlled variables are serving perception, their control is likely to optimize sensation [11,69,72–74].

Controlling hand speed in the current experiment resulted in maintaining the mean temporal frequency of fingertip activations (when crossing contour edges) between ~10 to 40 Hz across participants and sessions. In texture-related tasks the effective temporal frequency of individual receptor activation is typically maintained between 15 – 30 Hz [14]. This frequency range is optimal for activating rapidly-adapting (RA) receptors at the primate fingertip [41–43]. Emphasis of RA receptors in this experiment is in line with the fact that the height of our shapes was 25 microns, which is better sensed by RA receptors compared with SA receptors [42,43,62].

Our simulations further suggested that the JND-dependent control of scanning speed observed here (Fig. 5A) resulted in a quite uniform activation rate of RA receptors (Fig. 5B-C). Another support for the conjecture that the tactile system attempts to maintain uniform activation rates comes from our behavioral adaptation measurements. These results suggest that our participants made an effort to prevent receptor adaptation - participants with shorter adaptation times used curvier movements (Fig. 5F), which were likely to reduce receptor adaptation and thus maintain activation levels (Fig.5G). These results suggest the response

magnitude is also a controlled variable in planar shape perception. This suggests that the processing of sensory data in such cases assume a uniform response magnitude across neighboring receptors, presumably for allowing simple comparisons within and across the relevant receptor sheets.

Conclusion

Our high-resolution tracking of hand movements during planar shape perception revealed specific palpation strategies and specific relationships between the selected active palpation strategies and both the sensed shape and the idiosyncratic physiological thresholds of the participants. These results demonstrate the function of specific patterning of hand movements in tactile perception and provide insights into their origins.

MATERIALS AND METHODS

Overview of experimental design

This study was composed of two experiments. The first experiment (Experiment A) was designed to study the characteristics of tactile scanning when perceiving planar shapes. In the second experiment (Experiment B, conducted 18 months after Experiment A), we measured adaptation times and spatial resolutions of most (10 out of 11) of the participants who took part in Experiment A. The experimental procedures were approved by the Helsinki committee of the Tel Aviv Sourasky Medical Center.

Experiment A: Shape recognition

Participants: Eleven right-handed participants [seven female and four male students, aged 21-32, (25.36 ± 3.17) years] took part in the study. Informed consents were obtained from all participants, in accordance with the approved declaration of Helsinki for this project. The participants were paid for their participation. None of the participants had any previous experience with tactile recognition tasks.

Sample size: Sample size in this experiment is similar to the sample size used in previous works which aimed to characterize trajectories of hand motion [31,61,75–77]. Importantly, our sample (eleven subjects recorded for four or five sessions, total of 1196 trials) was sufficient for characterizing hand movement strategies and for studying their dependencies on the sensed shapes and on the measured physiological thresholds.

Experiment design and procedure: Participants were asked to identify two-dimensional (2D) engraved objects or features (Fig. 1B). Before the beginning of the first session, participants saw illustrations of all the objects or features that were presented in that session, and they were shortly trained by palpating on one of the objects or features until they reported that they understood the task. Participants performed four or five experimental sessions. The order of object presentation within each session was determined randomly, within one out of three possible presentation protocols (Supplementary material, Fig. 5). Whenever new shapes were introduced, a visual illustration of them was presented to participants at the start of the relevant session. At the beginning of each trial, the experimenter placed the participant's gloved-hand (Fig. 1A) a few centimeters above the center of the shape or feature board, and the trial began when the participant was allowed to put their hand on the shape (see 'Testing apparatus' below). Participants were requested to raise their palpating hand and name the shape placed in front of them when they identified it, as well as to report their confidence level. Trials ended with the participant's declaration or after a time limit of 30 seconds (sec) (whichever came first). A feedback was given on whether the answer was correct or not. In each session or block (see below), the order of trials was randomized and corrected such that each object was presented at least once. Trial presentation order within a session or block was kept constant across participants.

Presentation protocols: (Supplementary material, Fig. 5)

Session protocol I - Objects: During sessions I - III (20 trials each), five participants were presented with a fixed set of five geometrical objects (Fig. 1B, Set A, black). The order of trials was random but kept constant between participants. During session IV (34 trials) they were

presented with novel geometrical objects (Fig. 1B, Set B, blue). In each trial they performed a five-alternative forced choice (5-AFC) recognition task.

Session protocol II - Features: During sessions I - III (30 trials each), three participants were presented with a set of geometrical features (Fig. 1B, gray). Features were presented in three blocks, 10 trials each 'Angle' block (ninety, acute or obtuse angles), 'Tilt' block (tilt-right, tilt-left or straight vertical line) or 'Curvature' block (concave, convex or straight vertical line). Before each block, participants were notified which block is presented, and they were requested to name the presented feature in a three-alternative forced choice (3-AFC) recognition task. The order of blocks was randomized between participants and kept constant for each participant in all three sessions. The order of trials within each block was randomized but kept constant between participants. During session IV (34 trials) they were presented with novel geometrical objects (Fig. 1B, Set B, blue)

Session protocol III - Non fixed objects: During sessions I - V (35 trials each), three participants were presented with a non-fixed set of geometrical objects. During session I, the participants were presented with a set of five objects and during sessions II – V, one or two objects were replaced by novel ones (Supplementary material, Fig. 5, right, yellow). A visual illustration of the novel shapes were presented at the beginning of the session. The task gradually changed from a 5-AFC (session I) to a 9-AFC recognition task (session V; only five objects were presented in each session).

Hand tracking: Hand motion was tracked in 3D coordinates (x, y, z), using Vicon 612 motion capture system (Vicon Motion Systems Ltd, Oxford,.UK) and the Nexus 2.5 software. A custom 'Vicon labeling Skeleton Template' (VST) of the hand was designed. The VST included three segments and four markers attached above the wrist carpal bones and the middle finger's middle and proximal phalanges (Fig. 1A). At the beginning of each session, the VST was calibrated for the current subject's parameters, and a labeling skeleton file (VSK) was created. Hand motion was sampled at 200 Hz (76.5% of trials), 100 Hz (5.7%) and 240 Hz (17.8%), (see 'Vicon tracking' within 'Data Analysis' below).

Tactile shapes: Objects were engraved on aluminum boards of size 150X150 mm, such that the area inside the shape was raised to 25 μm in relation to the board surrounding. Shapes were divided into three sets: Objects – sets A & B (hereafter referred to as 'objects', Fig. 1B, black and blue) and Features set (Fig. 1B, gray).

Testing apparatus: Experiment took place in a Vicon arena. Participants sat in front of a table on which the stimulus was placed. The aluminum board was placed in a plastic frame, preventing its movement. Participants were blindfolded and wore a glove on their right hand. Four Vicon designated markers were connected to the glove, in a way that two markers were connected above the middle and proximal phalanges of the middle finger and two above the wrist carpal bones (Fig. 1A). In order to simplify and standardize the experiment, we reduced the degrees of freedom by banding together the index, middle and ring fingers with a tape- as if all three fingers belong to one surface plane. This restriction facilitated analysis and allowed comparison to other existing datasets. Three corresponding fingertips of the glove were cut, such that the finger pads were uncovered. Two glove sizes were used and chosen according to participant's hand size.

Data analysis: Vicon tracking: Trajectories of one marker were analyzed – the 'tip' marker that was placed above the middle finger, middle phalanges (closest to the finger pad, Fig. 1A). In a fraction of the sessions, the number of performed trials was smaller than planned (10 out of 47 sessions, 21.27%). A fraction of performed trials was excluded due to missing capture frames; the analysis throughout the paper includes the remaining number of trials (1196 out of 1367 trials, 87.4%). A fraction of these trials was not sampled at 200 Hz but at 100 Hz (5.7%) and 240 Hz (17.8%). These trials were resampled to 200 Hz: 100 Hz trials were linearly interpolated by a factor of two using the MATLAB function 'interp1'; 240 Hz trials were linearly interpolated by a factor of five using the 'interp1 'MATLAB function and then down sampled by a factor of six using the 'downsample' MATLAB function. In some sessions (n = 22 out of 47 sessions, 46.8%), the calibration of hand position in relation to the shape was lost .To compensate for differences in calibration quality, we chose for each session one trial with clear

449 hand-trajectory orientation relative to the borderlines of the shape and calculated the
450 translation and rotation between this trajectory and the shape. We used these parameters to
451 shift and rotate all the hand trajectories in that session.

452 Trial start, end and reaction time: At the beginning and end of each trial, participants lowered
453 or raised their hands, respectively (see experimental procedure). The point of hand lowering
454 was marked as the first frame in which the height in the z-axis was equal or smaller than the
455 median z height in the rest of the trial. The point of hand raising was marked in a similar way:
456 We smoothed hand velocities in the z-axis (using a moving average, MATLAB function,
457 'movmean', window size = 30 samples). A histogram of all data was plotted, forming a bi-
458 modal distribution. Hand raising was marked as the first frame in which z-speed was higher
459 than a threshold marking the second mode. In addition, in order to exclude 2D movements
460 that accompanied hand lowering or raising, trial start (t = 0) was defined as the first frame after
461 hand lowering in which the hand was at < 5 mm from the shape outline. Trial end was marked
462 as the last frame for which all consequent frames were > 5 mm from the contour. Trial reaction
463 time (RT) was the difference between trial start and trial end.

464 Classification of movement types: Following initial screening of trial trajectories, we aimed at
465 classifying the trials into two types: Contour-Following (*CF)* trials were defined as trials in
466 which the hand remained in the vicinity of the object outline. Scanning (*Sc*) trials were defined
467 as trials in which the trajectory crossed between distant parts of the objects' contour. Trials
468 were classified according to this distinction using two methods: Algorithmic and perceptual (by
469 human observers). The analysis throughout the paper is based on the algorithmic
470 classification. The human observer classification was used as a verification method. The
471 analyses based on it are presented as supplementary material (Supplementary material, Fig.
472 4).

473 *Algorithmic classification*: The algorithm used heuristic criteria that were based on our initial
474 inspections of motion strategies. For each original shape two similar "guiding shapes" were
475 plotted around its centroid: An inner and outer guiding shapes whose areas were 0.25 and 1.5

476 of the original shape, respectively. The 'L' and 'convex' objects were exceptional (see
477 Supplementary material, Fig. 4). Scanning trials (*Sc*) were trials in which either the hand
478 crossed the inner guiding shape (Fig. 2A, red, right top row), or those in which the hand did
479 not remain between the inner and outer guiding shapes for more than 75% of the time (Fig. 2A,
480 red, left, bottom row), or both (Fig. 2A, right, red, bottom row). *CF* trials (Fig. 2A, blue, top row)
481 were trials in which the hand remained in the buffer between the inner and outer guiding
482 shapes for more than 75% of the time, and did not cross the inner guiding shape.

483 *Human observer classification*: Two human observers classified the trials – one of the authors
484 (NM) and a naïve observer (SM). Each observer classified all trials twice consecutively, and
485 the second set of labeling was used for analysis. The observers could classify a trial as either
486 *CF*, *Sc* or *Oth*er. The two observers differed in the percentage of labeling trials as '*Other*' (NM,
487 11.8%; SM, 15.6%) and agreed on 66.6% of the trials (78% when *Other* trials were excluded).

488 Focal index**:** To evaluate the distribution of palpation density along the shapes' outlines, a
489 focal index was used. Circles at a radius of 10 mm were plotted on the object outline, such
490 that the distance between their centers was 0.5 mm. The traveled hand-trajectory distance in
491 each circle was computed. As a measure of dispersion, the difference in traveled distance
492 between the most visited (Fig. 3A, left, pink circle) and least visited (Fig. 3A, left, green circle)
493 areas was computed (Fig. 3A, right) and divided by their sum.

494 $$\boldsymbol{Focal\ index} = \frac{\mathbf{most\ visited} - \mathbf{least\ visited}}{\mathbf{most\ visited} + \mathbf{least\ visited}}$$

495 The least-visited circle was determined after removing circles that were not visited or circles
496 that overlapped with non-visited circles.

497 Similarity index: To quantify the spatiotemporal similarity of the motion trajectories in different
498 trials a similarity index was calculated for pairs of trials. For each pair, the trajectory of the
499 longer trial was down-sampled to match the length of the shorter trial, using the MATLAB
500 function 'resample'. Then, Pearson r was calculated separately for the horizontal (r_x) and
501 vertical (r_y) components of the two trajectories (Fig. 4A), and averaged:

$$\boldsymbol{Similarity\ index} = \frac{\mathbf{r}_x + \mathbf{r}_y}{\mathbf{2}}$$

The similarity index was computed for pairs of trajectories of the same subject exploring the same object (n = 7383 pairs, for all subjects and shapes), the same subject exploring different shapes (n = 61,004 pairs), and different subjects exploring the same shape (n = 41,700 pairs). In order to evaluate a null distribution of the similarity index (Fig. 4B), a normal distribution containing the possible values of the similarity index ($\pm$ 1) was created. The distribution had a mean zero and its $\pm$ 2.58 SD were equal to $\pm$ 1, respectively.

Trajectory curvature: Curvature evaluation was calculated in the following way: Each trial's hand trace was smoothed using a moving average with a window size of three samples. The trace was divided into segments of 20 mm length; the overlap between consequent segments was 0.01% (0.2 mm). Curvature index was defined as the subtraction of the shortest distance between the beginning and end of the segment's coordinates from the segment-traveled distance, divided by the traveled distance:

$$\boldsymbol{K\ segment} = \frac{\boldsymbol{traveld\ distance - shortest\ distance}}{\boldsymbol{traveld\ distance}}$$

The value of the curvature index is in the range between 0 to 1: The index is closer to zero as segment trace resembles a straight line (Fig. 5E, dark blue) and to one as it is more curved (Fig. 5E, dark red). The median of the indices of all segments in a trial was assigned as the trial curvature index. The constant-length segmentation was preferred over the constant-time segmentation because stronger curvatures are usually accompanied by slower movement [78,79], which would lead to over-estimation of curved movements in the latter case.

Trial entropy: In order to evaluate trajectories entropy, a gray scale image of each trial trajectory was created using the MATLAB function 'hist3'. The entire stimulus board (150x150 mm) was included. Bins with the size of 2x2 mm were used. The entropy of this grayscale image was calculated using the MATLAB function 'entropy'.

Visit rates: The number of visits of the hand's trajectory in each 2x2 mm bin were counted and divided by trial duration, and smoothed using the MATLAB function 'fspecial' with a averaging filter in the size of 2x2 mm.

Experiment B: Spatial and temporal thresholds

In this experiment, we tested the spatial resolution and effective adaptation time profiles of 10 of our participants.

Participants: Ten participants who participated in experiment-A took part in this experiment. The participants were naïve to the purpose of the experiment and were paid for their participation. Informed consents were obtained from all participants, in accordance with the approved Declaration of Helsinki for this project.

Task 1. Temporal profile of sensory adaptation

***Motion tracking*:** Trials were filmed (sampling frequency – 30 Hz) and were later analyzed using the MATLAB vision toolbox and the 'tracker' function.

Tactile objects: The 'straight' ,'right tilted' and 'convex' outlines from the features set were used (Fig. 1B, right, gray). In addition, we used eight identical-size rectangles raised to different heights, which were engraved on an aluminum board. Rectangle heights ranged from 10 μm to 80 μm and differed from one another by 10 μm.

Testing apparatus: Apparatus was identical to the apparatus in Experiment A, apart from the fact that it did not take place in the Vicon arena. The same glove was used, which had one polyester marker connected above the middle phalanges of the middle finger.

***Design and procedure*:** This experiment aimed to test the temporal profile of sensory adaptation while following the contour of our tactile objects. The participants were requested to use two types of motions: *Linear* and *Oscillating* (Fig. 2B). At the beginning of the session, these motions were demonstrated by the experimenter and then practiced by the participants, first on a desk and later using the 'rectangle' stimulus board (Fig. 1B, Set A, black). Before

553 each trial, participants were instructed which motion type they should use. After each trial, a
554 break of 45 sec was taken, in which participant's hand was placed such that the finger pads
555 were in the air. This was meant to allow full recovery of both slowly and rapidly adapting
556 receptors [80]. Before each trial, the participant's hand was placed on the starting point of
557 different outlines, and they were asked to report if they could feel the contour. Participants
558 were instructed to follow the contour using *Oscillating* or *Linear* motion until the experimenter
559 told them that the trial ended. Trial duration was 30 sec. During each trial, the contour was
560 tracked either once or more (moving back and forth along it), depending on hand velocity. The
561 participants were not asked to report anything nor were they given any feedback.

562 ***Stimuli Types :****Two tactile arrays were used:*

563 *Array with different outline types:* The outline was either 'straight', 'right tilted' or a 'convex'
564 engraved shapes raised to 25 μm (Fig. 1B, Features set, gray). This task included six trials,
565 as each outline type was followed using both motion types (*Oscillating* and *Linear*). The order
566 of the trials was random and kept constant between participants.

567 *Array with different outline heights*: A board with 8 rectangles was used. Rectangle lines
568 heights ranged from 10 μm to 80 μm and differed from one another by 10 μm. The task
569 included 16 trials, as each outline height was followed using both motion types. The task was
570 performed in two blocks - *Oscillating* and *Linear*. The order of blocks was random and kept
571 constant across participants. The order of trials within each block was randomized but kept
572 constant across participants.

573 ***Data analysis***

574 For each trial we identified the first time in which the tracking hand lost the outline using visual
575 inspection of the trial's movies. Two human observers examined the movies – one of the
576 authors (NM) and a naïve observer (SG). Each observer marked the first point in which the
577 hand's trajectory clearly deviated from the outline and assigned the time duration between trial
578 start and the point of deviation as the trial T_a (Supplementary material, Fig. 2F, left and second
579 left). In trials in which participants did not deviate from the outline the observers assigned T_a

as the maximal trial duration (30 sec, Supplementary material, Fig. 2F, right and second right). Trials in which it was not clear whether participants indeed lost the outline were excluded. For the majority of trials (n = 170 out of 225, 75.56%) both observers confidently assigned a T_a. For these trials, the correlations between the T_as assigned by the two observers, for *Oscillating* and *Linear* motion trials, were r = 0.73 and r = 0.68, respectively ($p<0.005$, Supplementary material, Fig. 2G, left and middle). The distribution of the differences between the two observers' T_as exhibited a clear mode at 0 and a secondary mode between 0 to 5 sec (Supplementary material, Fig. 2G, right). In this analysis we included only trials for which the difference was < 5 sec, which composed 86.47% (147 out of 170) of the trials. For these trials, the T_a was taken as the mean of both observers' T_as.

Task 2. Spatial resolution

The spatial just-noticeable difference (JND) of each participant was measured using a static two-point discrimination test, applied to the pads of index, middle and ring fingers, similar to a procedure previously described [58]. Participants placed their hand comfortably on a table and were blindfolded. Participants were asked to report whether they feel contact in one or two points on their skin. The task was demonstrated on the participants' forearm before starting the experiment. An adjustable compass was used. The interval between the two tips of the compass was gradually reduced until the participant could not differentiate between the two points. An effort was made by the experimenter to keep the same amount of pressure. Threshold was determined as the first interval at which the two points could not be distinguished. The order of measured fingers was ring, middle and index finger for all participants.

Assessment of the participants' spatial tactile resolution: The reliability of the two points discrimination method in assessing spatial tactile resolution had been debated [60,81]. We have thus examined the dependency of the correlation of our participants' speed with their spatial tactile resolution (as shown in Fig.5A) on the method used to assess the latter. We considered

two such methods – our JND assessment and a grating orientation task [60]. We used the limits of agreement between two-points discrimination and grating orientation task thresholds (Mean $_{methods\ difference}$=0 mm, 95% limits of agreement = ± 1 mm, [47]) for a bootstrap testing. At each iteration (n = 1,000), each participant's JND was added a value randomly picked from the distribution of differences between the two methods. Correlation was tested between speed and adjusted JNDs values. The thousand iterations allowed us to assess the confidence range (Fig. 5A) for the correlation of participants' speed with their spatial tactile resolution.

Statistical analysis - experiments A & B

Unless stated otherwise, the compared distributions were tested for normality using the Anderson-Darling test. If at least one of the compared distributions was recognized as non-normal, the Mann–Whitney U test (non-paired comparisons, two tailed), or Wilcoxon signed rank test (paired comparisons, two tailed) were used. Otherwise, a two-tailed (independent or paired) t-test was used. Categorical data was tested using the Chi-square test of independence using all of the trials in each protocol session (84-146 trials). Multiple comparisons were corrected using the Bonferroni method. Since in some of the compared distribution part of the observations were dependent (trials belonging to the same subject), significance was additionally tested using bootstrap. Unless stated otherwise, all significance reports are based on both a model-based (one of the aforementioned) and a bootstrap test.

Bootstrap was performed in the following way: Trials from both of the compared groups were mixed to one pool. Ten thousand iterations were used. At each iteration, two samples were taken from the mixed pool. One sample was at the size of the number of trials of comparison group I and the second at the size of the number of trials of group II. A difference calculation was repeated for each iteration. The fraction of bootstrap values that were more extreme (larger or smaller, depending on the case) than the experimental one was reported as the boundary of the probability of getting the experimental value by chance. In order to verify that the three sessions protocols were not different in terms of their kinematics, median values of

compared kinematics (tangential speed, focal, curvature and similarity indices) were examined using the Kruskal-Wallis test.

Simulations

Relation between speed and spatial resolution: To test the effects of JND-dependent speed modulations on neuronal activations, simulations of mechanoreceptor responses were performed using TouchSim [49]. In order to simulate fingers with different receptors spacing, five grids of rapidly-adapting (RA) mechanoreceptive units were formed. These grids varied in the inter-receptor distances (2 to 4 mm, with 0.5 mm intervals). The resulting grid sizes were in the size of 10.5 x 10.5 and 12.5 x 12.5 mm (Supplementary material, Fig. 2E, left). Grids were created using the TouchSim built-in function 'affpop grid'. JND values larger than 4 mm created grids with smaller number of neurons (9 versus 16-49 neurons) and smaller dimensions (9x9 and 10x10 mm) and were therefore not used. The stimulus was comprised of two columns of pins, aligned between the two left-most receptor columns (Supplementary material, Fig. 2E, right). The pin radius was 0.5 mm. In order to simulate different scanning speeds, in each simulation run, the two stimulus columns were pressed onto the finger grid with a delay that corresponded to the simulated scanning speed. Scanning speed was varied between 20 to 250 mm/sec (with intervals of 10 mm/sec) and pressing duration was 0.2 sec. The duration of each simulation was 1 sec, and the sampling rate was 5000 Hz. Default parameters of the model were used to determine the stimulus indentation depth: indentation was implemented as a sine wave with an amplitude varying between 0.5 to 1.5 mm. The resulting spike counts per each grid in all tested speed values were smoothed (moving average, window size = 5 samples).

Differences between *Linear* and *Oscillating CF:* The effect of *Linear* and *Oscillating CF* (Fig.2B) on receptors activations was tested. A grid of RA units with 1 mm receptors spacing and in the size of 12.5 x 12.5 mm was formed (Supplementary material, Fig. 2E, left). The stimulus was comprised of one column of pins, aligned between the two left-most receptor

columns (Supplementary material, Fig. 2E, right). Pin radius was 0.5 mm. In order to simulate *Linear CF*, the pins were pressed one after another. To simulate *Oscillating CF*, every 0.25 sec, pins pressing was stopped for 0.2 sec. The stop in pin pressing aimed to mimic the deviation from the contour. Default parameters of the model were used to determine the stimulus indentation depth: indentation was implemented as a sine wave with an amplitude varying between 0.5 to 1.5 mm. The duration of the simulation was 2 sec and the sampling rate was 5000 Hz.

REFERENCES

1. Ahissar, E. & Arieli, A. Figuring space by time. *Neuron* (2001) doi:10.1016/S0896-6273(01)00466-4.

2. Brecht, M. *et al.* The neurobiology of Etruscan shrew active touch. *Philosophical Transactions of the Royal Society B: Biological Sciences* (2011) doi:10.1098/rstb.2011.0160.

3. Cole, G. G. Active vision: the psychology of looking and seeing. J. M. Findlay and I. D. Gilchrist. *Appl. Cogn. Psychol.* (2004).

4. Diamond, M. E., Von Heimendahl, M., Knutsen, P. M., Kleinfeld, D. & Ahissar, E. 'Where' and 'what' in the whisker sensorimotor system. *Nat. Rev. Neurosci.* **9**, 601–612 (2008).

5. Halpern, B. P. Tasting and smelling as active, exploratory sensory processes. *Am. J. Otolaryngol. Neck Med. Surg.* **4**, 246–249 (1983).

6. Kleinfeld, D., Ahissar, E. & Diamond, M. E. Active sensation: insights from the rodent vibrissa sensorimotor system. *Curr. Opin. Neurobiol.* **16**, 435–444 (2006).

7. Land, M. F. Eye movements and the control of actions in everyday life. *Prog. Retin. Eye Res.* **25**, 296–324 (2006).

8. Lederman, S. J. & Klatzky, R. L. Hand movements: A window into haptic object recognition. *Cogn. Psychol.* (1987) doi:10.1016/0010-0285(87)90008-9.

9. Rucci, M., Ahissar, E. & Burr, D. Temporal Coding of Visual Space. *Trends Cogn. Sci.* 22, 883–895 (2018).

689 10. Schroeder, C. E., Wilson, D. A., Radman, T., Scharfman, H. & Lakatos, P. Dynamics
690 of Active Sensing and perceptual selection. *Current Opinion in Neurobiology* (2010)
691 doi:10.1016/j.conb.2010.02.010.

692 11. Ahissar, E. & Assa, E. Perception as a closed-loop convergence process. *Elife* **5**, 1–
693 26 (2016).

694 12. Bensmaia, S. J. & Hollins, M. The vibrations of texture. *Somatosens. Mot. Res.* **20**,
695 33–43 (2003).

696 13. Cascio, C. J. & Sathian, K. Temporal cues contribute to tactile perception of
697 roughness. *J. Neurosci.* **21**, 5289–5296 (2001).

698 14. Gamzu, E. & Ahissar, E. Importance of Temporal Cues for Tactile Spatial- Frequency
699 Discrimination. *J. Neurosci.* **21**, 7416–7427 (2001).

700 15. Hollins, M. & Bensmaïa, S. J. The coding of roughness. *Can. J. Exp. Psychol.* **61**,
701 184–195 (2007).

702 16. Katz, D. *The World of Touch*. *The World of Touch* (Psychology Press, 2013).
703 doi:10.4324/9780203771976.

704 17. Saig, A., Gordon, G., Assa, E., Arieli, A. & Ahissar, E. Motor-Sensory Confluence in
705 Tactile Perception. *J. Neurosci.* **32**, 14022–14032 (2012).

706 18. Weber, A. I. *et al.* Spatial and temporal codes mediate the tactile perception of natural
707 textures. *Proc. Natl. Acad. Sci. U. S. A.* (2013) doi:10.1073/pnas.1305509110.

708 19. Gibson, J. J. Observations on active touch. *Psychol. Rev.* (1962)
709 doi:10.1037/h0046962.

710 20. Klatzky, R. L. & Balakrishnan, J. D. Task-driven extraction of object contour by human
711 haptics: Part 2. *Robotica* **9**, 179–188 (1991).

712 21. Lederman, S. J. & Balakrishnan, J. D. Task-driven extraction of object contour by
713 human haptics: Part 1. *Robotica* (1991) doi:10.1017/S0263574700015551.

714 22. Nelinger, G., Assa, E. & Ahissar, E. Tactile object perception. *Scholarpedia* **10**, 32614
715 (2015).

716 23. Drewing, K. After experience with the task humans actively optimize shape
717 discrimination in touch by utilizing effects of exploratory movement direction. *Acta*
718 *Psychol. (Amst).* **141**, 295–303 (2012).

719 24. Lezkan, A. & Drewing, K. Interdependences between finger movement direction and

720 haptic perception of oriented textures. *PLoS One* **13**, 1–25 (2018).

721 25. Withagen, A., Kappers, A. M. L., Vervloed, M. P. J., Knoors, H. & Verhoeven, L. The
722 use of exploratory procedures by blind and sighted adults and children. *Attention,*
723 *Perception, Psychophys.* **75**, 1451–1464 (2013).

724 26. Ahissar, E. & Vaadia, E. Oscillatory activity of single units in a somatosensory cortex
725 of an awake monkey and their possible role in texture analysis (tactile
726 sensation/phase-locked loop/corticothalamic loop/pattern recognition). *Neurobiology*
727 **87**, 8935–8939 (1990).

728 27. Buckley, C. L. & Toyoizumi, T. A theory of how active behavior stabilises neural
729 activity: Neural gain modulation by closed-loop environmental feedback. *PLoS*
730 *Comput. Biol.* **14**, 370–372 (2018).

731 28. Marken, R. S. You Say You Had a Revolution: Methodological Foundations of Closed-
732 Loop Psychology. *Rev. Gen. Psychol.* **13**, 137–145 (2009).

733 29. Riley, M. A., Wagman, J. B., Santana, M. V., Carello, C. & Turvey, M. T. Perceptual
734 behavior: Recurrence analysis of a haptic exploratory procedure. *Perception* **31**, 481–
735 510 (2002).

736 30. Saraf-Sinik, I., Assa, E. & Ahissar, E. Motion Makes Sense: An Adaptive Motor-
737 Sensory Strategy Underlies the Perception of Object Location in Rats. *J. Neurosci.*
738 **35**, 8777–8789 (2015).

739 31. Smith, A. M., Gosselin, G. & Houde, B. Deployment of fingertip forces in tactile
740 exploration. *Exp. Brain Res.* **147**, 209–218 (2002).

741 32. Noton, D. & Stark, L. Scanpaths in saccadic eye movements while viewing and
742 recognizing patterns. *Vision Res.* (1971) doi:10.1016/0042-6989(71)90213-6.

743 33. Foulsham, T. & Underwood, G. What can saliency models predict about eye
744 movements? Spatial and sequential aspects of fixations during encoding and
745 recognition. *J. Vis.* (2008) doi:10.1167/8.2.6.

746 34. Hacisalihzade, S. S., Stark, L. W. & Allen, J. S. Visual Perception and Sequences of
747 Eye Movement Fixations: A Stochastic Modeling Approach. *IEEE Trans. Syst. Man*
748 *Cybern.* (1992) doi:10.1109/21.155948.

749 35. Holm, L. & Mäntylä, T. Memory for scenes: Refixations reflect retrieval. *Mem. Cogn.*
750 (2007) doi:10.3758/BF03193500.

751 36. Underwood, G., Foulsham, T. & Humphrey, K. Saliency and scan patterns in the

752 inspection of real-world scenes: Eye movements during encoding and recognition.
753 *Vis. cogn.* (2009) doi:10.1080/13506280902771278.

754 37. Noton, D. & Stark, L. Scanpaths in eye movements during pattern perception. *Science*
755 *(80-.).* (1971) doi:10.1126/science.171.3968.308.

756 38. Damiano, C. & Walther, D. B. Distinct roles of eye movements during memory
757 encoding and retrieval. *Cognition* (2019) doi:10.1016/j.cognition.2018.12.014.

758 39. Hollins, M. & Risner, S. R. Evidence for the duplex theory of tactile texture perception.
759 *Percept. Psychophys.* **62**, 695–705 (2000).

760 40. Abraira, V. E. & Ginty, D. D. The sensory neurons of touch. *Neuron* (2013)
761 doi:10.1016/j.neuron.2013.07.051.

762 41. Ahissar, E. Temporal-Code to Rate-Code Conversion by Neuronal Phase-Locked
763 Loops. *Neural Comput.* (1998) doi:10.1162/089976698300017683.

764 42. Johansson, R. S., Landström, U. & Lundström, R. Responses of mechanoreceptive
765 afferent units in the glabrous skin of the human hand to sinusoidal skin
766 displacements. *Brain Res.* **244**, 17–25 (1982).

767 43. Talbot, W. H., Darian-Smith, I., Kornhuber, H. H. & Mountcastle, V. B. The sense of
768 flutter-vibration: comparison of the human capacity with response patterns of
769 mechanoreceptive afferents from the monkey hand. *J. Neurophysiol.* (1968)
770 doi:10.1152/jn.1968.31.2.301.

771 44. Darian-Smith, I. & Oke, L. E. Peripheral neural representation of the spatial frequency
772 of a grating moving across the monkey's finger pad. *J. Physiol.* (1980)
773 doi:10.1113/jphysiol.1980.sp013498.

774 45. Peters, R. M., Hackeman, E. & Goldreich, D. Diminutive digits discern delicate details:
775 Fingertip size and the sex difference in tactile spatial acuity. *J. Neurosci.* **29**, 15756–
776 15761 (2009).

777 46. Zoeller, A. C. & Drewing, K. A Systematic Comparison of Perceptual Performance in
778 Softness Discrimination with Different Fingers. *Attention, Perception, Psychophys.*
779 (2020) doi:10.3758/s13414-020-02100-4.

780 47. Bruns, P. *et al.* Tactile acuity charts: A reliable measure of spatial acuity. *PLoS One*
781 (2014) doi:10.1371/journal.pone.0087384.

782 48. Carr, C. E. Processing of temporal information in the brain. *Annual Review of*
783 *Neuroscience* (1993) doi:10.1146/annurev.ne.16.030193.001255.

784 49. Saal, H. P., Delhaye, B. P., Rayhaun, B. C. & Bensmaia, S. J. Simulating tactile
785 signals from the whole hand with millisecond precision. *Proc. Natl. Acad. Sci. U. S. A.*
786 **114**, E5693–E5702 (2017).

787 50. Wong, M., Peters, R. M. & Goldreich, D. A physical constraint on perceptual learning:
788 Tactile spatial acuity improves with training to a limit set by finger size. *J. Neurosci.*
789 **33**, 9345–9352 (2013).

790 51. Callier, T., Saal, H. P., Davis-Berg, E. C. & Bensmaia, S. J. Kinematics of
791 unconstrained tactile texture exploration. *J. Neurophysiol.* **113**, 3013–3020 (2015).

792 52. Vega-Bermudez, F., Johnson, K. O. & Hsiao, S. S. Human tactile pattern recognition:
793 Active versus passive touch, velocity effects, and patterns of confusion. *J.*
794 *Neurophysiol.* **65**, 531–546 (1991).

795 53. Brandt, S. A. & Stark, L. W. Spontaneous eye movements during visual imagery
796 reflect the content of the visual scene. *J. Cogn. Neurosci.* (1997)
797 doi:10.1162/jocn.1997.9.1.27.

798 54. Morash, V. S., Connell Pensky, A. E. & Miele, J. A. Effects of using multiple hands
799 and fingers on haptic performance. *Perception* **42**, 759–777 (2013).

800 55. Fish, J. & Soechting, J. F. Synergistic finger movements in a skilled motor task. *Exp.*
801 *Brain Res.* **91**, 327–334 (1992).

802 56. Hager-Ross, C. & Schieber, M. H. Quantifying the independence of human finger
803 movements: Comparisons of digits, hands, and movement frequencies. *J. Neurosci.*
804 **20**, 8542–8550 (2000).

805 57. Ross, H. E. & Murray, D. J. *E.H. Weber on the tactile senses, (2nd Edition)*. *E.H.*
806 *Weber on the Tactile Senses, (2nd Edition)* (2018). doi:10.4324/9781315782089.

807 58. Louis, D. S. *et al.* Evaluation of normal values for stationary and moving two-point
808 discrimination in the hand. *J. Hand Surg. Am.* **9**, 552–555 (1984).

809 59. Weinstein, S. Intensive and extensive aspects of tactile sensitivity as a function of
810 body part, sex and laterality. in *First International Symposium on Skin Senses* (1968).

811 60. Johnson, K. O. & Phillips, J. R. Tactile spatial resolution. I. Two-point discrimination,
812 gap detection, grating resolution, and letter recognition. *J. Neurophysiol.* (1981)
813 doi:10.1152/jn.1981.46.6.1177.

814 61. Zilbershtain-Kra, Y., Graffi, S., Ahissar, E. & Arieli, A. Active sensory substitution
815 allows fast learning via effective motor-sensory strategies. *iScience* **24**, 101918

(2021).

62. Neubarth, N. L. *et al.* Meissner corpuscles and their spatially intermingled afferents underlie gentle touch perception. *Science (80-.).* (2020) doi:10.1126/science.abb2751.

63. Severson, K. S. *et al.* Active Touch and Self-Motion Encoding by Merkel Cell-Associated Afferents. *Neuron* (2017) doi:10.1016/j.neuron.2017.03.045.

64. Marken, R. S. Controlled variables: Psychology as the center fielder views it. *Am. J. Psychol.* (2001) doi:10.2307/1423517.

65. Gruber, L. Z. & Ahissar, E. Closed loop motor-sensory dynamics in human vision. *PLoS One* (2020) doi:10.1371/journal.pone.0240660.

66. Rao, R. P. N. & Ballard, D. H. Predictive coding in the visual cortex: A functional interpretation of some extra-classical receptive-field effects. *Nat. Neurosci.* (1999) doi:10.1038/4580.

67. Barascud, N., Pearce, M. T., Griffiths, T. D., Friston, K. J. & Chait, M. Brain responses in humans reveal ideal observer-like sensitivity to complex acoustic patterns. *Proc. Natl. Acad. Sci. U. S. A.* (2016) doi:10.1073/pnas.1508523113.

68. Huang, Q. & Luo, H. Saliency-based rhythmic coordination of perceptual predictions. *J. Cogn. Neurosci.* (2019) doi:10.1162/jocn_a_01371.

69. Biswas, D. *et al.* Closed-Loop Control of Active Sensing Movements Regulates Sensory Slip. *Curr. Biol.* (2018) doi:10.1016/j.cub.2018.11.002.

70. Burstedt, G. K. O., Birznieks, I., Edin, B. B. & Johansson, R. S. Control of forces applied by individual fingers engaged in restraint of an active object. *J. Neurophysiol.* **78**, 117–128 (1997).

71. Todorov, E. & Jordan, M. I. Optimal feedback control as a theory of motor coordination. *Nat. Neurosci.* **5**, 1226–1235 (2002).

72. Buckley, C. L. & Toyoizumi, T. A theory of how active behavior stabilises neural activity: Neural gain modulation by closed-loop environmental feedback. *PLoS Comput. Biol.* (2018) doi:10.1371/journal.pcbi.1005926.

73. Eldridge, S. & von Uexkull, J. Theoretical Biology. *J. Philos.* (1928) doi:10.2307/2014622.

74. Simony, E., Saraf-Sinik, I., Golomb, D. & Ahissar, E. *Sensation-Targeted Motor*

Control: Every Spike Counts? Focus on: “Whisker Movements Evoked by Stimulation of Single Motor Neurons in the Facial Nucleus of the Rat”. *J. Neurophysiol.* **99**, 2757–2759 (2008).

75. Lezkan, A. *et al.* Multiple Fingers - One Gestalt. *IEEE Trans. Haptics* (2016) doi:10.1109/TOH.2016.2524000.

76. Morash, V. S. Systematic Movements in Haptic Search: Spirals, Zigzags, and Parallel Sweeps. *IEEE Trans. Haptics* (2016) doi:10.1109/TOH.2015.2508021.

77. Yan, Y., Goodman, J. M., Moore, D. D., Solla, S. A. & Bensmaia, S. J. Unexpected complexity of everyday manual behaviors. *Nat. Commun.* (2020) doi:10.1038/s41467-020-17404-0.

78. Viviani, P. & Schneider, R. A Developmental Study of the Relationship Between Geometry and Kinematics in Drawing Movements. *J. Exp. Psychol. Hum. Percept. Perform.* **17**, 198–218 (1991).

79. Viviani, P. & Flash, T. Minimum-jerk, two-thirds power law, and isochrony: converging approaches to movement planning. *J. Exp Psychol. Hum. Percept. Perform* **21**, 32–53 (1995).

80. Leung, Y. Y., Bensmaïa, S. J., Hsiao, S. S. & Johnson, K. O. Time-Course of Vibratory Adaptation and Recovery in Cutaneous Mechanoreceptive Afferents. *J. Neurophysiol.* **94**, 3037–3045 (2005).

81. Tong, J., Mao, O. & Goldreich, D. Two-point orientation discrimination versus the traditional two-point test for tactile spatial acuity assessment. *Front. Hum. Neurosci.* (2013) doi:10.3389/fnhum.2013.00579.

Acknowledgements: We thank Nir Knaan and Yahel Zamosh for helping in designing and conducting experiment A and Silman Bensmaia for insightful comments and advices. This research received funding from the European Research Council (ERC) under the EU Horizon 2020 Research and Innovation Programme (grant agreement No 786949). E.A. holds the Helen Diller Family Professorial Chair of Neurobiology. A.A. holds the Sam and Frances Belzberg Chair in Memory and Learning

Authors contributions:

N.M: Designed experiment, performed experiment, analyzed data,wrote the paper.

878 G.N: Designed experiment, performed experiment, analyzed data,wrote the paper.

879 E.A: Designed experiment, wrote the paper.

880 A.A: Designed experiment, wrote the paper.

881 **Declaration of interests:** The authors declare no competing interests.

Figures

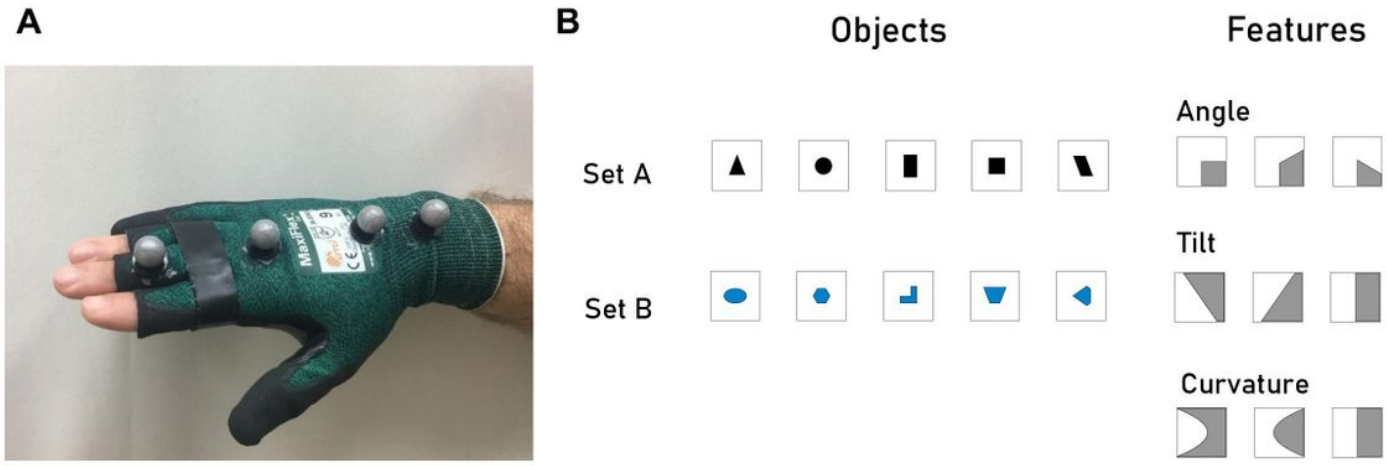

Figure 1

Please see the Manuscript PDF file for the complete figure caption

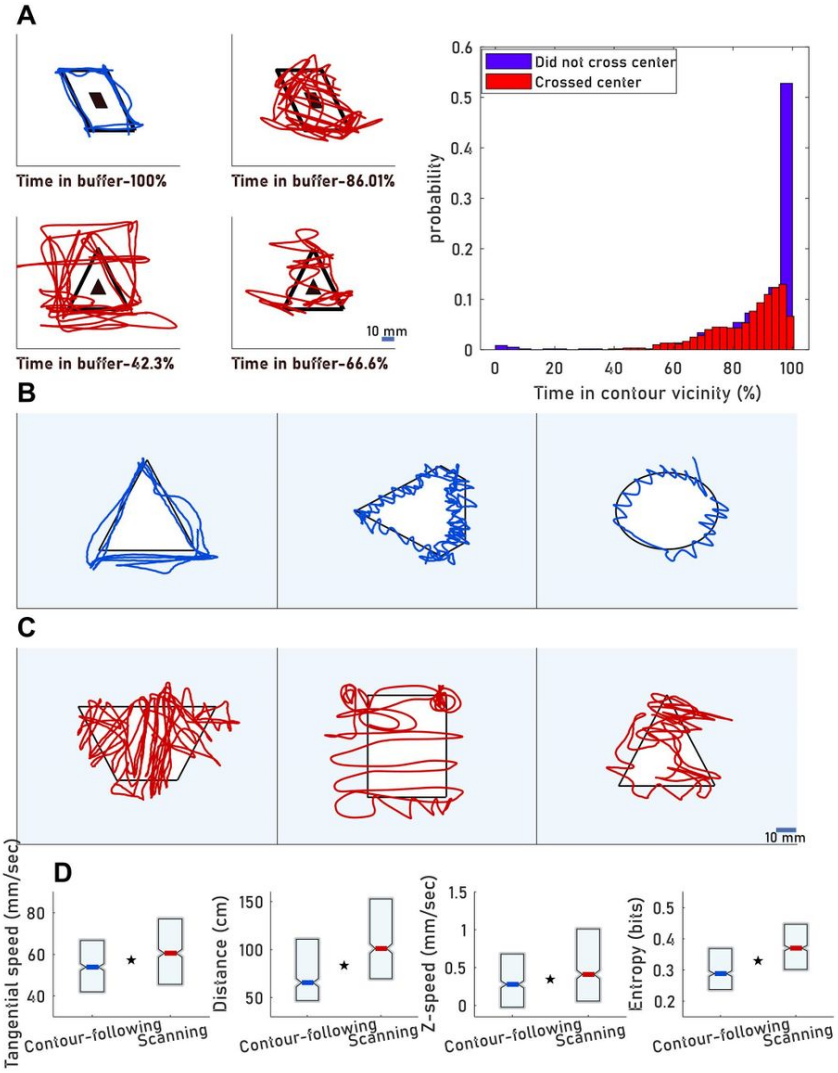

Figure 2

Please see the Manuscript PDF file for the complete figure caption

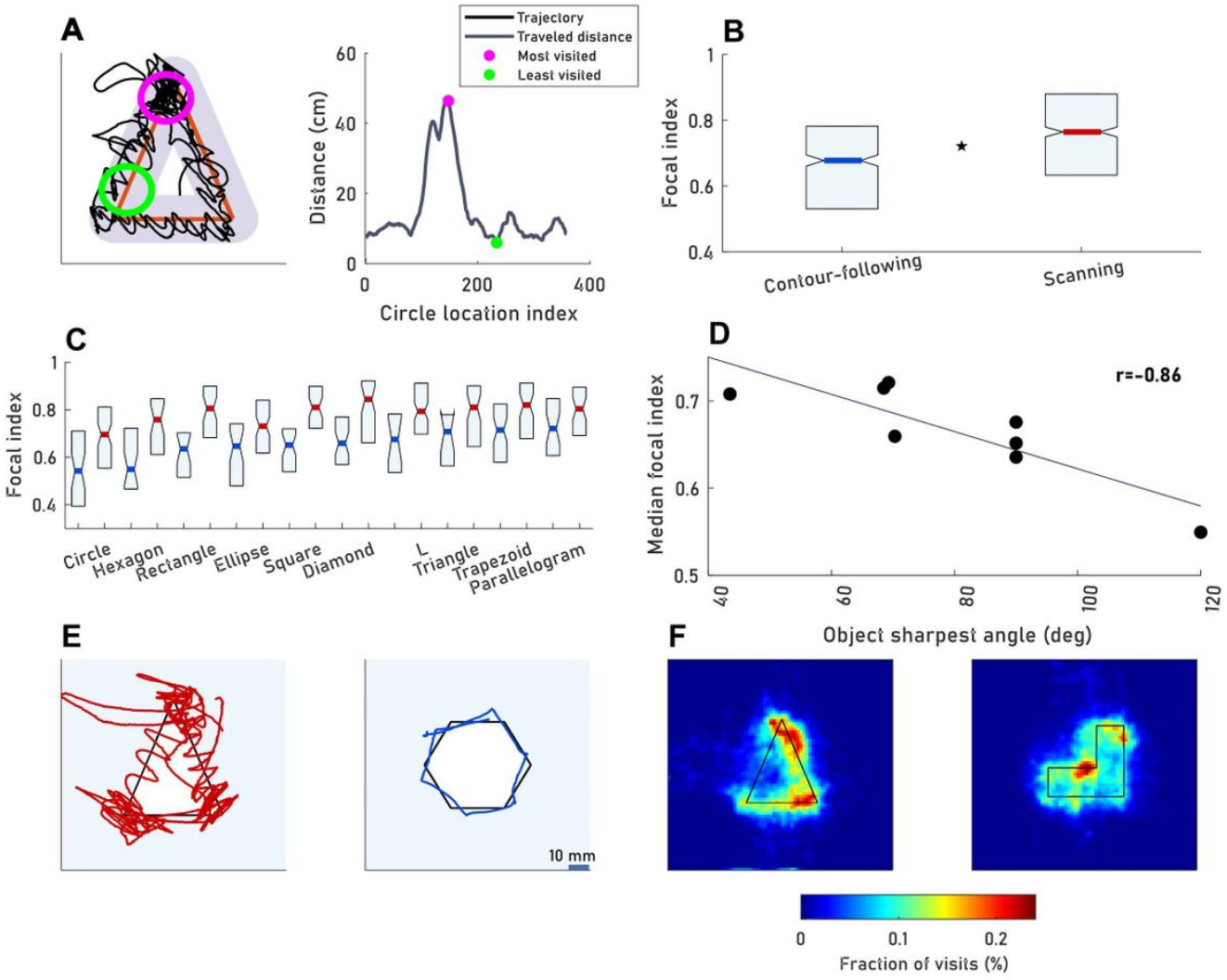

Figure 3

Please see the Manuscript PDF file for the complete figure caption

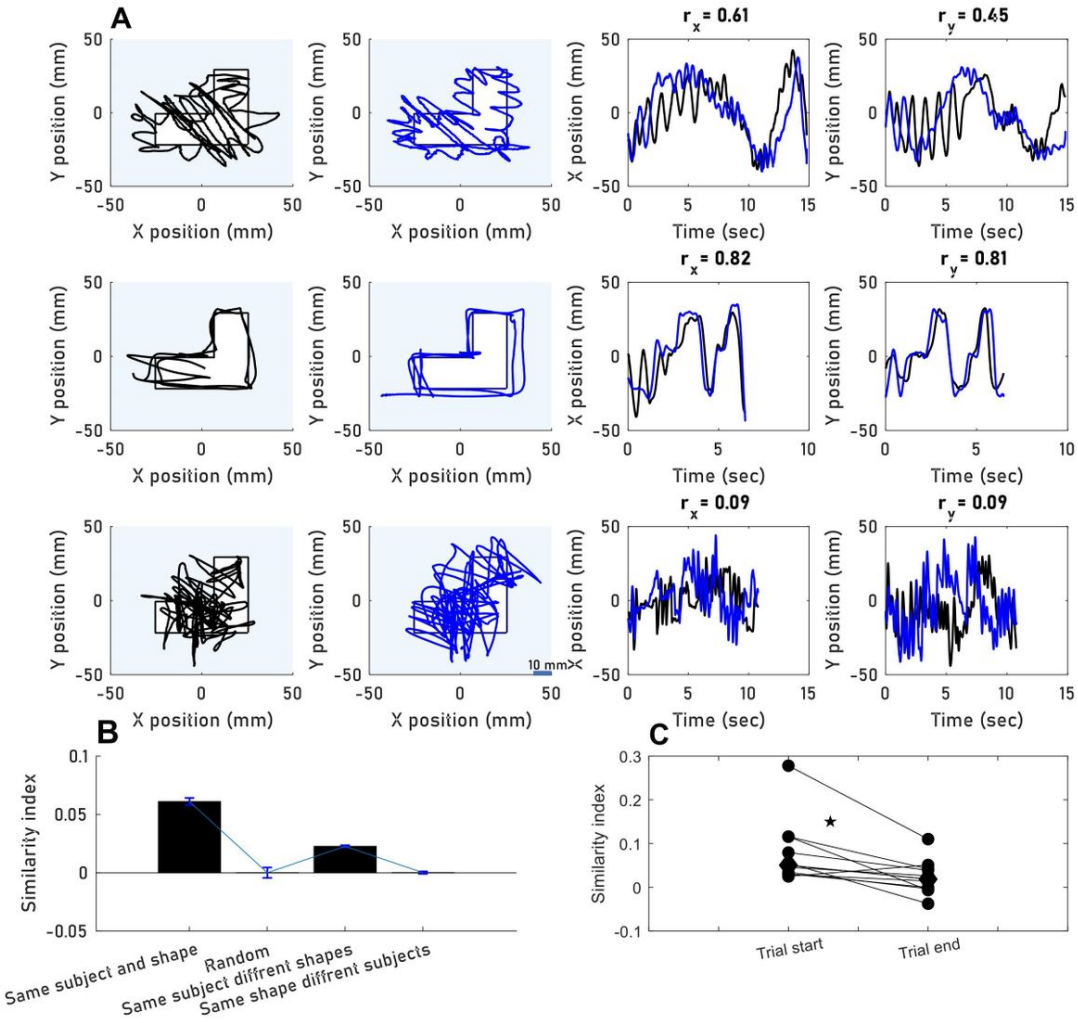

Figure 4

Please see the Manuscript PDF file for the complete figure caption

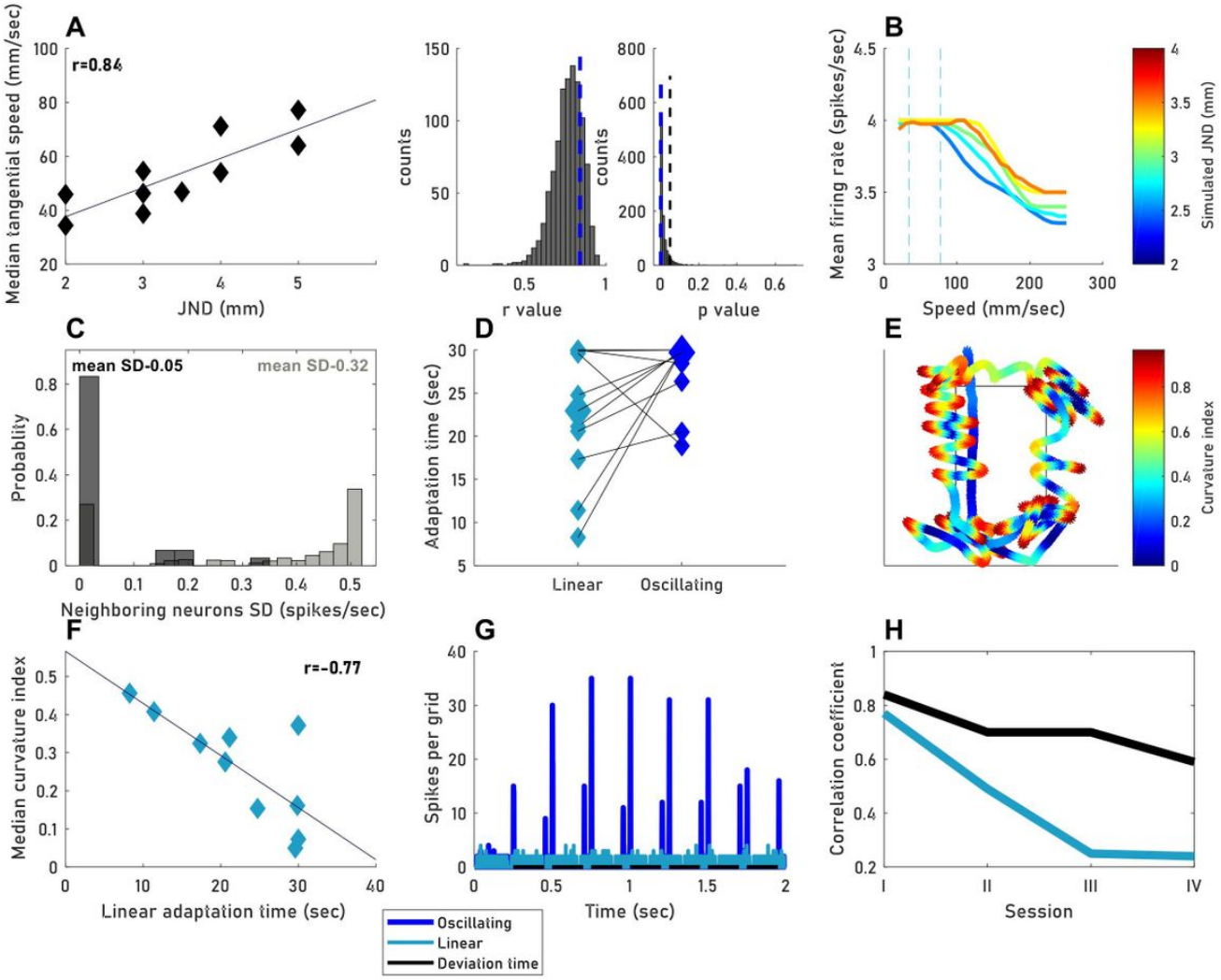

Figure 5

Please see the Manuscript PDF file for the complete figure caption

Supplementary Files

This is a list of supplementary files associated with this preprint. Click to download.

- SupplementarymaterialIdiosyncraticfunctionsofactivetouchstrategiesinshapeperceptionNeomiMizrachiGuyNelingerEhudAhissarAmosArieli.pdf